

**Ultrafast X-ray tomographic imaging of multiphase flow in bubble columns – Part 2
Characterisation of bubbles in the dense regime**

Lau, Y. M.; Möller, F.; Hampel, U.; Schubert, M.

DOI

[10.1016/j.ijmultiphaseflow.2018.02.009](https://doi.org/10.1016/j.ijmultiphaseflow.2018.02.009)

Publication date

2018

Document Version

Final published version

Published in

International Journal of Multiphase Flow

Citation (APA)

Lau, Y. M., Möller, F., Hampel, U., & Schubert, M. (2018). Ultrafast X-ray tomographic imaging of multiphase flow in bubble columns – Part 2: Characterisation of bubbles in the dense regime. *International Journal of Multiphase Flow*, 104, 272-285. <https://doi.org/10.1016/j.ijmultiphaseflow.2018.02.009>

Important note

To cite this publication, please use the final published version (if applicable).
Please check the document version above.

Copyright

Other than for strictly personal use, it is not permitted to download, forward or distribute the text or part of it, without the consent of the author(s) and/or copyright holder(s), unless the work is under an open content license such as Creative Commons.

Takedown policy

Please contact us and provide details if you believe this document breaches copyrights.
We will remove access to the work immediately and investigate your claim.



Ultrafine gradient microstructure induced by severe plastic deformation under sliding contact conditions in copper

Carlos Gabriel Figueroa^a, Rafael Schouwenaars^{b,c,*}, Jacinto Cortés-Pérez^a, Roumen Petrov^{c,d}, Leo Kestens^{c,d}

^a Centro Tecnológico Aragón, Facultad de Estudios Superiores Aragón, Universidad Nacional Autónoma de México, Av. Rancho Seco s/n, Col. Impulsora, Cd. Nezahualcóyotl 57130, Estado de México, Mexico

^b Departamento de Materiales y Manufactura, Facultad de Ingeniería Edificio O, Universidad Nacional Autónoma de México, Avenida Universidad 3000, Coyoacán 04510, México D.F., Mexico

^c Metal Science and Technology Group, EEMMeCS Department, Ghent University, Technologiepark 903, 9052 Zwijnaarde (Ghent), Belgium

^d Department of Materials Science and Engineering, Delft University of Technology, Mekelweg 2, 2628 CD Delft, The Netherlands

ARTICLE INFO

Keywords:

Sliding contact
Copper
Severe plastic deformation
Grain refinement
Recrystallisation
Nanohardness

ABSTRACT

Sliding contact induces severe plastic deformation (SPD) at the surface of ductile materials and induces a microstructural gradient associated to a significant increase of hardness toward the surface. This gradient allows observing all stages of grain refinement in SPD, as illustrated here by the analysis of polycrystalline electrolytic copper tested in a coaxial tribometer. Materials tested in the cold-rolled state and after annealing were characterised by high-resolution electron backscattering diffraction and nano-indentation. The incremental plastic strain produces an ultrafine microstructure in the top layers, which gradually changes to the original size in unaffected material. In cold-rolled material, an intermediate recrystallised layer is observed. The separation of the Misorientation Angle Distribution (MAD) in a low-angle portion and a high angle portion allows characterising the accumulation of strain induced misorientation, while the Kernel Average Misorientation (KAM) provides information on the evolution of substructure at the finest levels. The results point toward a process where strain-induced effects compete continuously with recrystallisation, except for the surface layer in the cold-rolled material, where dynamic recrystallisation is dominant. Combining the information from KAM and sub-grain size distribution, the measured hardness can be explained as a combination of grain size and dislocation hardening.

1. Introduction

When ductile materials are subject to sliding wear conditions, strong microstructural modifications are observed close to the surface. One of these modifications is the formation of a tribolayer with a thickness between several hundreds of nanometres to tens of microns [1], depending on the contact conditions and the initial microstructure [2]. Rigney [3–5] explained the formation of the tribolayer as the combination of severe plastic deformation (SPD), mechanical mixing (MM) and material transfer. Kapoor [6–8] described the corresponding SPD-process as the accumulation of small plastic strains due to cyclic loading, unlike most common SPD process in which the total strain is achieved in a few cycles of very large plastic strains [9–11]. It has been suggested that tribolayers are responsible for a decrease in wear rate and friction coefficient in sliding contact of metals [12–14]. The technological importance of this process has been illustrated by studies on

bearings [15], railway tracks [16–19], brake disks [20,21], journal bearings [22] and ceramic materials [23–25].

The effect of SPD on tribological behaviour has been reported for low carbon steel, titanium and copper [26–29]. This improvement is often attributed to the proposal by Archard [30], in which wear resistance is proportional to the material hardness. Nevertheless, this empirical relation is overly simple, suggesting the need for a combination of ductility and strength. Such a combination may be obtained by introducing a gradient microstructure by superficial SPD methods like surface mechanical grinding treatment (SMGT) [31,32], surface mechanical attrition treatment (SMAT) [33] or platen friction sliding deformation (PFSD) [34].

Since grain size is a key microstructural factor affecting the mechanical behaviour of polycrystalline metals, the interest for developing new processing techniques, which allow modifying grain size without changing composition has increased. An attractive method for

* Corresponding author at: Metal Science and Technology Group, EEMMeCS Department, Ghent University, Technologiepark 903, 9052 Zwijnaarde (Ghent), Belgium.

E-mail addresses: raf_schouwenaars@yahoo.com (R. Schouwenaars), jacop@unam.mx (J. Cortés-Pérez), Roumen.Petrov@UGent.be (R. Petrov), Leo.Kestens@UGent.be (L. Kestens).

producing ultrafine-grained and nanostructured materials is SPD, due to the possibility to enhance the strength up to a factor of eight in pure metals and by 30–50% for alloys [35,36]. Using a combination of high hydrostatic pressure and shear deformation, the straining is practically unlimited while the shape of the part is almost constant [37,38].

The grain refinement by SPD in high or medium stacking fault energy (SFE) materials like Fe, Al or Cu is due to the formation of a dislocation-based substructure. This refinement is more pronounced at low or medium strains, while in later straining stages, grain boundary misorientation increases [39–42], leading to the formation of predominantly high angle grain boundaries (HAGB) in materials with accumulated strains above 6 to 8 [11,43]. The evolution from a homogeneous dislocation forest to elongated dislocation cells and subsequently sub-grains with increasing plastic strain has been described extensively in several review papers [44–46]. A quantitative analysis of the increment of subgrain boundary misorientation, and hence their evolution from LAGB to HAGB has been provided by Pantleon & Hansen [47] and Pantleon [48].

An alternative viewpoint is that ultrafine grained structures obtained by SPD at relatively low temperatures are produced by continuous dynamic recrystallization (CDRX) which is characterised by a slower kinetics than conventional dynamic recrystallization (DRX) because of the requirement of large strains ($\epsilon > 3$) [49]. In CDRX new grains form during deformation as a result of the continuous accumulation of dislocations increasing the sub-boundary misorientation, producing a gradual transformation from low angle grain boundaries (LAGB) into HAGB [49–51]. The grain refinement in ultrafine or nanostructured metals increases the mechanical strength, combined with the effect of work hardening by increasing dislocation density [43]. Although a significant decrease in ductility is expected and often observed, it has been reported that UFG materials produced by SPD sometimes show a good combination of strength and toughness [43,52–54].

Although in most known SPD techniques like High Pressure Torsion (HPT) or Equal Channel Angular Pressing (ECAP) the material flow is more complex than in a classical torsion test, it is assumed that the deformation mode is simple shear [55,56]. The crystallographic texture obtained in torsion tests on face centred cubic (FCC) metals has been extensively studied [57–60]. Two fibres and one component are observed: the A-fibre $\{111\}\langle uvw \rangle$, B-fibre $\{hkl\}\langle 110 \rangle$ and the C-component $\{100\}\langle 110 \rangle$ [34]. Ideal orientations associated to the mentioned fibres have been defined based on simulation and experimental data; these orientations are shown in Table 1, in which $\{hkl\}\langle uvw \rangle$ refers to the set of planes and directions parallel to the shear plane and shear direction respectively.

In previous research, the superficial modification in Cu, Al-Sn, and Cu-Mg-Sn systems was analysed, showing the influence of annealing in the tribological behaviour and the formation of tribolayers in two-phase

Table 1
Ideal texture components observed in FCC materials subject to simple shear [58,61,62].

Component	$\{hkl\}\langle uvw \rangle$	ϕ_1	Φ	Φ_2
A	$\{1\bar{1}\bar{1}\}\langle 110 \rangle$	0	35.26	45
\bar{A}	$\{\bar{1}11\}\langle \bar{1}\bar{1}0 \rangle$	180	35.26	45
A^*	$\{\bar{1}\bar{1}1\}\langle 112 \rangle$	35.37	45	0
		125.37	90	45
\bar{A}^*	$\{11\bar{1}\}\langle 112 \rangle$	144.74	45	0
		54.74	90	45
B	$\{\bar{1}12\}\langle 110 \rangle$	0	54.74	45
		120	54.74	45
\bar{B}	$\{1\bar{1}\bar{2}\}\langle \bar{1}\bar{1}0 \rangle$	60	54.74	45
		180	54.74	45
C	$\{100\}\langle 110 \rangle$	90	45	0
		0	90	45
A fiber $\{111\}\langle uvw \rangle$				
B fiber $\{hkl\}\langle 110 \rangle$				

alloys [29,63]. In the present work, a coaxial tribometer developed by the authors [64] was used to modify the surface of pure copper, inducing a microstructural gradient which allows for a systematic study of the microstructure, texture evolution and their interrelation with hardness and grain size. The microstructure and texture were analysed by means of detailed EBSD scans along the cross section to the worn surface, while nano-hardness measurements were performed in the previously scanned zones.

2. Materials and Methods

Commercial slabs of electrolytic tough pitch copper with purity of 99.9% were cold rolled to a final reduction of 88% equivalent to a Von Mises strain of $\epsilon_{VM} = 2.5$ and subsequently annealed at 873 K for 45 min. The material was tested under two different conditions: cold rolled (CuCR) and recrystallized (CuRX). The surface modification was conducted at room temperature using a coaxial tribometer [64]. The experiment consists in the application of a constant normal load of 100 N by means of a cylindrical pin of AISI9840 steel with a spherical cap of radius equal to 200 mm in contact with the surface of a Cu-coupon of 20 mm \times 20 mm. The pin rotates on its own axis for 300 s at a constant angular speed of 60 rpm. Before the tribological test, Cu surfaces were prepared by conventional mechanical polishing to a mean square roughness of 0.62 μm and 0.64 for CuCR and CuRX respectively. Based on the mechanical work dissipated in system and considering the aluminium sample holder as an infinite heat sink, it can be calculated that the temperature increase in the Cu-coupon is $< 1^\circ\text{C}$.

The sample reference system follows the traditional rolling convention, representing the rolling direction as RD, transversal direction as TD and normal direction as ND. The worn surface is taken perpendicular to ND. Samples for microstructure analysis were taken perpendicular to TD, which for this observation plane is also the sliding direction. Transverse sections through the centre of the wear track were prepared by conventional mechanical polishing and analysed unetched on a FEI Quanta 450-FEGSEM operating at 20 kV with spot size of 5, corresponding to a beam current of 2.4 nA. TSL-OIM Data collection version 6.2 was used to acquire EBSD patterns, the working distance was 20 mm with a tilt angle of 70° . Step size used for coarse-grained and cold-rolled zones was 0.1 μm , while for the layer closest to the worn surfaces it was 55 nm, in hexagonal grid scan mode.

EBSD scans were performed to analyse the microstructural gradient from top of the wear-affected zone to a zone where the original microstructure was evident. To ensure the statistical validity of data, the size of the areas analysed was varied according to the grain size. The orientation data were post-processed with MTEX [65] quantitative texture software analysis version 4.0.23. A clean-up procedure to eliminate pixels with neighbour confidence index correlation < 0.1 was performed before the microstructural and textural analysis. To define grains, a cut-off angle of 5° was considered for the minimum boundary misorientation in LAGB and 15° for HAGB.

KAM was calculated for the six nearest neighbours of each pixel (excluding grain boundaries) with threshold of 3° . This parameter quantifies small local differences in orientation which are not identified as LAGB under the threshold mentioned before. KAM therefore indicates the presence of local lattice bending due to dislocation structures which are not otherwise resolved. The grain boundary misorientation angle distribution (MAD) was obtained from the experimental data. A frequency distribution was obtained by fitting an 8th degree polynomial to the empirical distribution function of measured grain boundary misorientation and calculating the derivative. The polynomial was forced to be equal to 0 and 1 at the lowest and highest misorientation in the dataset, respectively, with derivative equal to 0 in both points. Twin boundaries were excluded from the calculation. A theoretical MAD was calculated from the measured texture, rather than using the classical Mackenzie distribution which is valid for random textures. This calculated “random” MAD represents a

random distribution of grain boundaries in a non-random texture, i.e. the non-correlated misorientation distribution as defined by Toth et al. [65].

A broad peak is often present in the MADs for low misorientations. The low-angle portion was defined by subtracting the measured MAD from the calculated one and selecting only the points from zero to the first zero crossing of this difference. In agreement to theoretical calculations by Pantleon [47,66], this part of the distribution was fitted by Rayleigh and Maxwell distributions, with the latter giving a significantly better fit. A weighted sum of the Maxwell fit with the calculated MAD was then made to minimise the square difference. This procedure allows for a qualitative assessment of the presence of low-angle grain boundaries as well as deviations from randomness in the high-angle portion of the distribution.

Nano-hardness measurements were conducted in the same zone as studied by EBSD. Indentations were made by means of a Berkovich indenter adapted to a Bruker Innova atomic force microscope. The maximum applied load was 120 μN with a holding time of 10s. 5 indents were made at each given depth with a lateral spacing of 5 μm . Sampling depths were spaced at 20 μm , with smaller steps close to the surface and larger steps in the unaffected zone. Post-indentation scans were made in tapping mode and analysed using Bruker NanoScope analysis software version 1.4. Contact depth was calculated using the Oliver and Pharr method [68,69], whereas the pile up correction was performed by means of the semi-ellipse method described by Kese and co-workers [70–72].

3. Results

3.1. Characterisation of the Starting Material

The initial texture and microstructure for the cold-rolled and the recrystallised materials are presented in Fig. 1. Fig. 1a presents a typical cold rolled structure. In CuRX (Fig. 1b), it is possible to observe a near random distribution of orientations with average grain size of 5.0 μm and 51% of $\Sigma 3$ boundaries (twins). The orientation density function (ODF) calculated for initial conditions in CuCR (Fig. 2b) shows the α -fibre ($\langle 011 \rangle // \text{ND}$) dominated by Goss ($\{011\} \langle 001 \rangle$) and Brass ($\{001\} \langle 211 \rangle$) as well as Copper ($\{112\} \langle 111 \rangle$) and S ($\{123\} \langle 614 \rangle$), connected by the β -fibre. As expected for the annealed material, the ODF for CuRX (Fig. 2c) shows a strong Cube ($\{001\} \langle 100 \rangle$) component and a less intense Q ($\{013\} \langle 231 \rangle$) component, whereas the β -fiber observed is retained from rolling texture.

3.2. Modification of CuRX

Fig. 3 shows results for CuRX after the tribological test. IPFMs along the vertical gradient of the material (Fig. 3a) illustrate the microstructural evolution along the ND-RD plane, MAD in Fig. 3b and KAM in Fig. 3c.

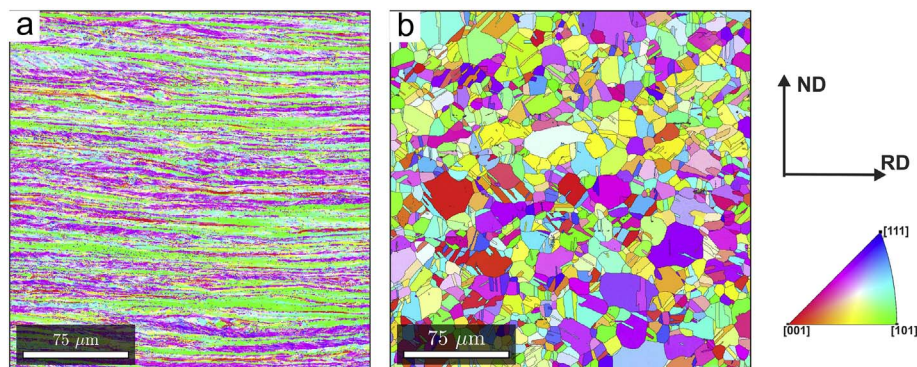


Fig. 1. Inverse pole figure maps (IPFM) of the starting materials. (a) CuCR, (b) CuRX.

The microstructure observed in the zone corresponding to 10 μm below the surface has an average grain size of 500 nm and shows a predominance of HAGB with misorientation between 30° – 40° . Further away from the worn surface, the average grain size gradually increases and the GBM distribution changes, as illustrated by the zone marked as 45 μm , where the average grain size is 700 nm and the increment in the LAGB indicates a dislocation substructure within the grains. At 100 μm the highest fraction of LAGBs is found, which then gradually decreases until reaching the original microstructure with a classical recrystallisation texture and 51% of $\Sigma 3$ boundaries. The KAM of the zones marked as 10 μm , 45 μm and 100 μm are all similar and indicate a higher density of dislocations than in the zone without modification.

(111) Pole figures of CuRX are shown in Fig. 4. The zone between 5 μm to 20 μm (Fig. 4a) is characterised by the A and B partial fibres with a maximum at A*. At increasing depth, these fibres are better defined, in spite of a decrease of the maximum intensity at A* (Fig. 4b). In Fig. 4c, which corresponds to a distance of 60 μm to 80 μm from the surface, the cube orientation is dominant and the β -fibre starts to appear, in a transition toward the initial texture (Fig. 4e). The transition from the annealing texture at the bottom toward the cube dominated texture is accompanied by the decrease of identifiable twins because of straining and the subsequent grain fragmentation.

The onset of this phenomenon is illustrated by the IPFM at 240 μm shown in Fig. 5. The microstructural change in this zone is characterised by an increment in dislocation density, creating orientation gradients within the grains. Another characteristic of the strained material are the bended twins marked in Fig. 5. The bended twins show an internal orientation spread suggesting that, as deformation increases, twins fragmentate and gradually disappear, as illustrated by the disappearance of the $\Sigma 3$ boundaries (Fig. 3b) and the increasing dominance of the near-cube orientation (Fig. 4d). As the twins disappear from the microstructure (see Fig. 3a, 100 μm below the surface), the β -fiber vanishes as well, as seen in Fig. 4d.

3.3. Modification of CuCR

Fig. 6 shows the results for CuCR. Closest to surface, the plastic deformation produced an UFG structure with equiaxial grains with average grain size of 250 nm. The MAD is characteristic of random orientations dominated by HAGB, as expected in UFG materials obtained by SPD [72]. This distribution shows good correspondence with the Mackenzie distribution, with the exception for a hump in the range of small angles, which indicates that a certain fraction of LAGBs is still present. With increasing distance from the surface, a gradual increase in grain size is observed. At 55 μm from the surface, the average grain size is 800 nm and a larger fraction of LAGBs is found, although HAGBs still dominate. At 130 μm from the surface, the morphology is more like cold rolled material but with differences in grain orientations. Large orientation spread within individual grains is characteristic for a deformation substructure. The latter agrees with the GBM which shows

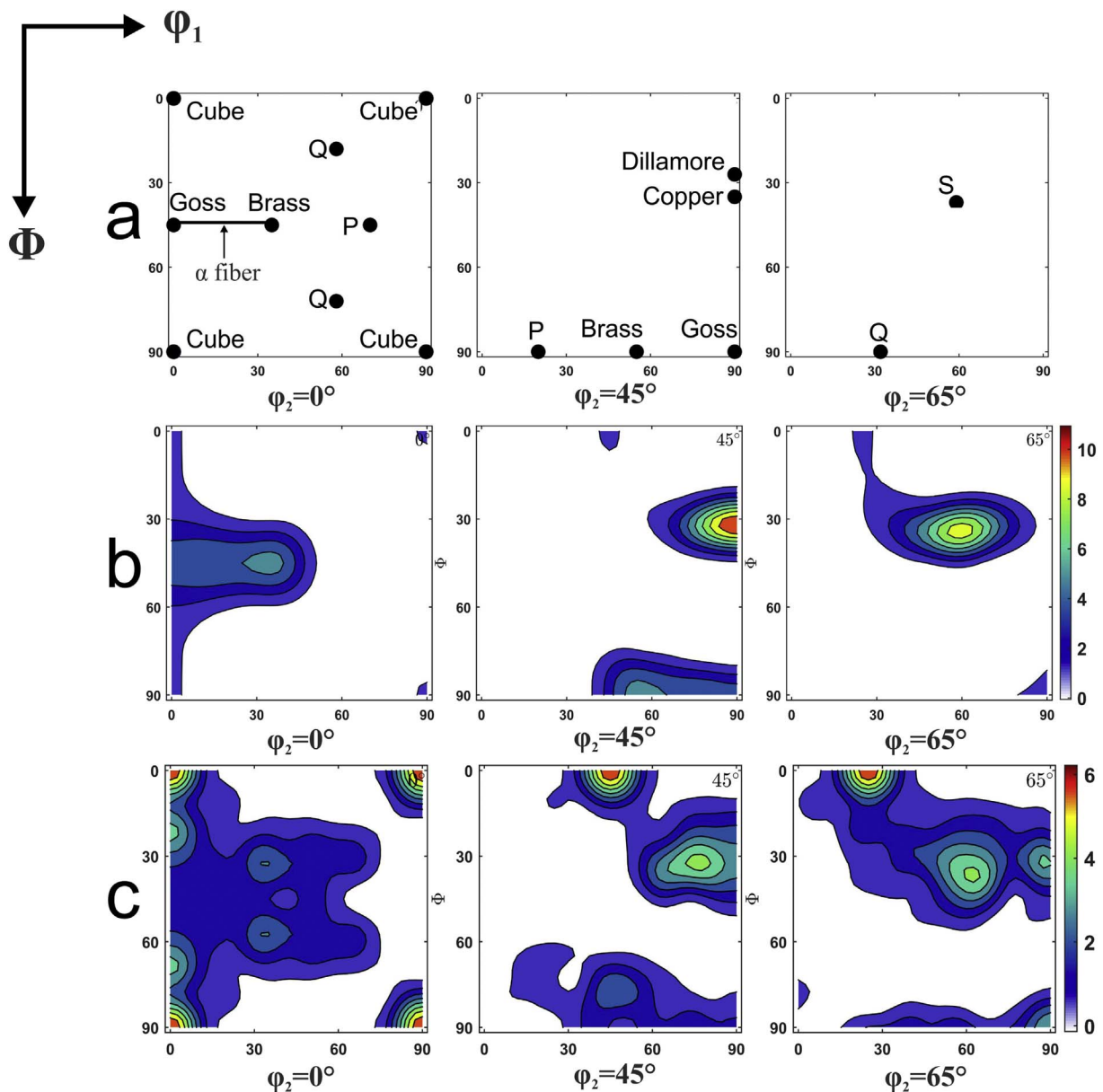


Fig. 2. ODF sections ($\phi_2 = 0^\circ, 45^\circ, 65^\circ$) of the starting materials. (a) Main components observed in FCC materials, (b) CuCR, (c) CuRX.

the highest frequency between 5° – 15° , corresponding to LAGB associated to strained grains with high dislocation density and an increase of the KAM. In the maps at 65 and $130\ \mu\text{m}$ bands of near-cube orientation appear, which can be interpreted in terms of the partial recrystallisation of the cold-rolled material due to the additional driving force induced by the imposed deformation. At $200\ \mu\text{m}$ from the surface, the original cold rolled structure is evident.

Fig. 7 shows a set of (111) PF corresponding to the EBSD measurements. Fig. 7a shows the PF of the zone between 5 and $20\ \mu\text{m}$ from the worn surface. The partial fibres usually seen in torsion textures are present ($A\{111\}\langle uvw \rangle$, $B\{hkl\}\langle 110 \rangle$) with $I_{\text{max}} = 2.24$ corresponding to the A^* orientation. Between 20 and $50\ \mu\text{m}$ below the worn surface (Fig. 7b) the A-fibre is no longer observed and the maximum intensity has increased, due to the lower shear strain in this zone. The increase in intensity continues at 50 – $80\ \mu\text{m}$ below the worn surface (Fig. 7c) a near-cube ($\{001\}\langle 100 \rangle$) texture (rotated with respect to ND), which is commonly associated to a recrystallized microstructure obtained by annealing a FCC cold rolled material. This texture gradually modifies into the β -fibre typically observed in FCC cold rolled materials, corresponding to the layer where no microstructural modification was

observed (Fig. 7e). It shall be noted that even in this zone, a small rotation with respect to the ideal cube orientation is found, indicating a long-range shear strain field extends into the zone in which the microstructural modification is no longer evident. The hypothesis that the observed rotation could be due to specimen misalignment was verified and could be rejected.

Fig. 8 compares the texture indices (TI) for CuCR and CuRX. The difference between both initial conditions is substantial, with a high TI in CuCR and a lower TI CuRX, which is explained by the high density of $\Sigma 3$ boundaries, as twinning reduces the strength of the preferred orientations. A higher TI is seen in CuRX in the zone from 100 to $140\ \mu\text{m}$, corresponding to the disappearance of the twins. In CuCR, TI drops significantly in the surface zone, where the shear texture is more strongly developed and the grain size is smallest. It is known that as effect of rigid body rotations, the orientations in simple shear are not stable, this provokes that simple shear texture are usually weak [73,74]. However, a pronounced drop in TI is observed in CuCR and not in CuRX, which is a point to be addressed in the discussion.

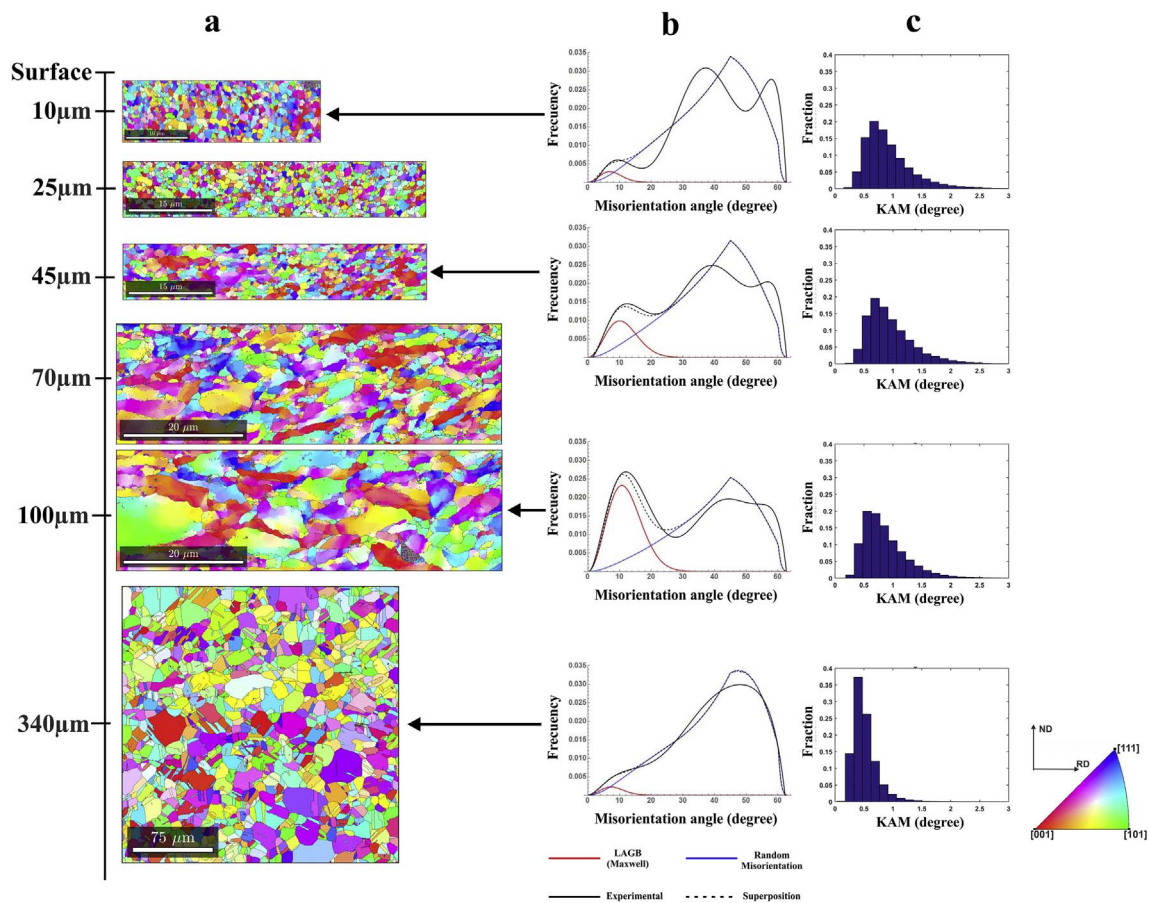


Fig. 3. Microstructural evolution along the ND-RD plane after the tribological test of CuRX. (a) IPFM, (b) Grain boundary misorientation distribution, (c) Kernel average misorientation. The vertical distance bar is not to scale.

3.4. Nanohardness and Grain Size

The evolution of hardness and grain size with respect to the distance from the surface are shown in Fig. 9a. Nano-hardness values of CuCR are relatively constant with exception for the ultrafine zone close to the surface. The softening observed 120 μm below the surface can be associated to partial recrystallisation, as evidenced also by the cube-type texture and the microstructure of this zone. In CuRX a monotonous increase of the hardness is observed with an increasing gradient toward the surface. The hardness in the fully developed shear zone is slightly lower than in CuCR, which corresponds also to a slightly larger grain size.

The grain size gradient is most easily described in CuRX, which has a constant large grain size down to approximately 250 μm from the surface and then shows a gradual refinement to 500 nm at the surface. In CuCR, it is difficult to objectively define the grain size of the original material, due to the strongly elongated structure and the abundance of LAGB. From the partially recrystallised layer toward the surface, grain size is well-defined and decreases monotonically to a minimum diameter of 250 nm.

The relation between hardness and grain size is shown in a Hall-Petch plot (Fig. 9b). Although the grain size effect is evident, it clearly does not obey the Hall-Petch relationship in a strict sense. The absence of a clear trend over the entire range of grain sizes can be explained by the complex interaction between dislocation hardening, LAGBs and HAGBs, with the latter defining the grain size but all three contributing to hardening.

4. Discussion

From the results presented in the previous section, it is seen that the sliding wear tests on copper offer the opportunity for studying all stages of severe plastic deformation along the deformation gradient of the worn samples, from zero strain in the substrate to very high deformations at the surface. The two different initial conditions (cold rolled and recrystallised) provide complementary information about the mechanisms which are active in this process.

Several interesting results can be pointed out from the start. First, there is the drop in hardness and texture index at the surface of CuCR. Second, the grain boundary misorientation distributions for CuCR at 55 μm and CuRX at 10 μm are very similar. Third, the KAM of CuCR closest to the surface is similar to the KAM of CuRX in the unaffected zone, while the KAM of CuRX in the surface zone is similar to the KAM of CuCR in the unaffected zone.

The main questions to be addressed in this context are the role of strain in the substructure and microstructure modification and the role of recrystallisation which may occur as a consequence and in conjunction with the applied strain. To present these topics within the appropriate context, it is useful to briefly discuss the mechanical aspects of the tribological process.

4.1. Tribomechanics

The texture results (Figs. 4 and 7) clearly indicate that the strain mode at the surface is simple shear, from the analogy to reported results on torsion and HPT tests [57–60,62]. However, from the microstructures shown in Figs. 3 and 6, it may be deduced that an outward flow of the material is also present in the intermediate layer. This radial

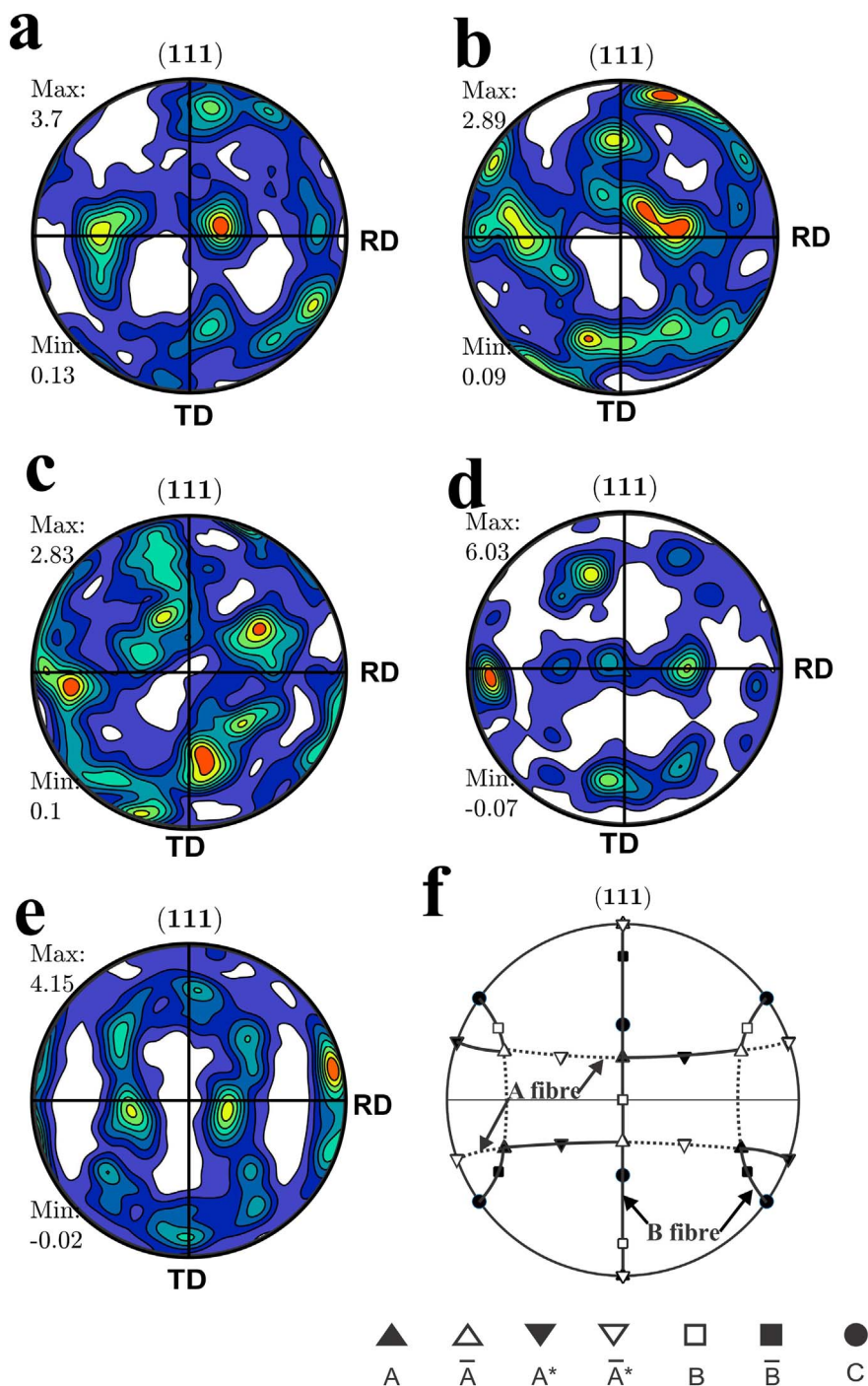


Fig. 4. (111) PF of CuRX after the tribological test. (a) 5–20 μm from the worn surface, (b) 40–60 μm, (c) 60–80 μm, (d) 100–140 μm, (e) 240–440 μm, (f) ideal orientations of a simple shear texture.

flow is indispensable to explain the formation of wear tracks without weight loss as observed in a previous study [64]. It is also interesting to notice that the plastic strain field extends beyond the zone where microstructural modification is visually identifiable. This is evidenced by the rotation of the textures with respect to ND as compared with the ideal textures for cold rolled or recrystallised copper. The long-range plastic strain field is too small to cause significant crystal rotation or grain shape modification, but is observed in the form of a rigid body rotation.

Within the field of tribology, it is accepted that the observed strains are induced gradually by incremental plastic strain. The strain is induced by the cyclic loading of the substrate, where each cycle induces

small increments of plastic strain (ratchetting) [6,8,75]. Under the present experimental conditions, where the load is constantly applied in a circular contact zone, it is understood that the smooth irregularities (asperities) on the contacting body are responsible for the formation of small-amplitude plastic waves in the contact zone [76]. While in earlier reports, the number of cycles responsible for the phenomenon was in the order of magnitude of millions [6,22], here, only 300 cycles were applied, although in each cycle many asperities may move over a single spot. Hence, the present conditions are somewhere between the ones encountered in real-world tribological applications on the one hand and classical SPD processes on the other. In the latter, only a small number of cycles with very high strain are applied.

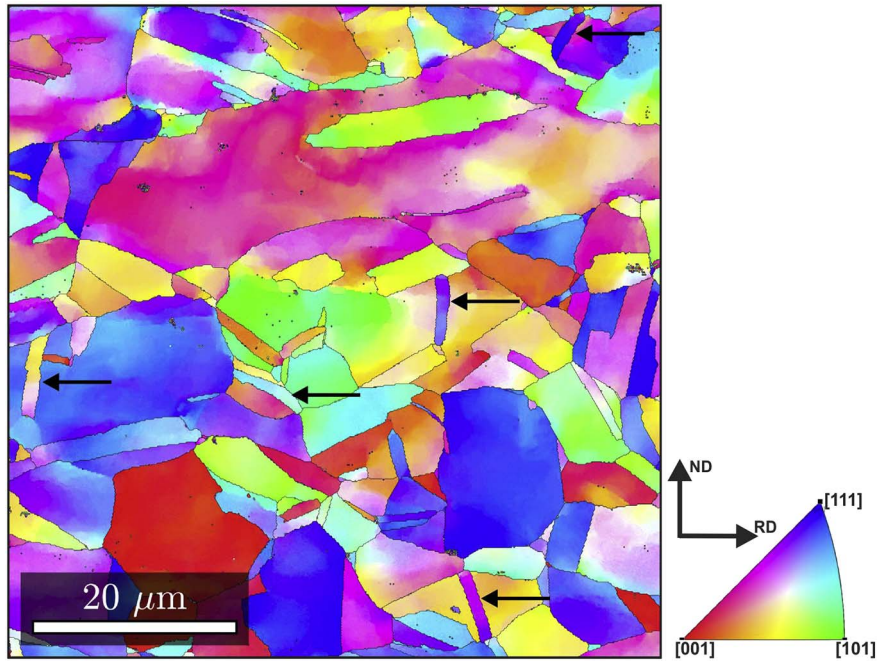


Fig. 5. Zone 140 μm under the worn surface showing strained grains with high dislocation density. Arrows point out twins which are bended as consequence of plastic deformation.

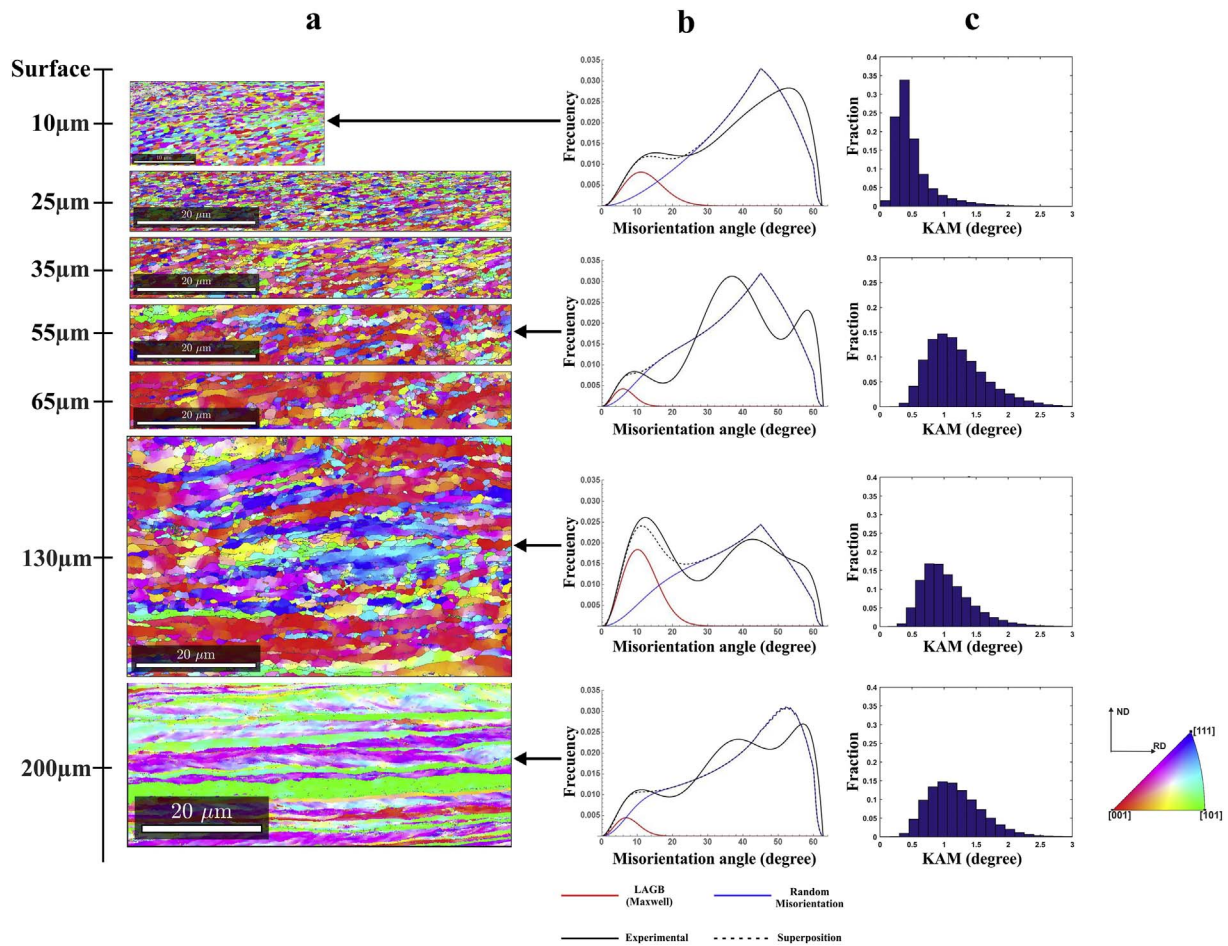


Fig. 6. Microstructural evolution along the ND-RD plane after the tribological test of CuCR. (a) IPFM, (b) Grain boundary misorientation distribution, (c) Kernel average misorientation. The vertical distance bar is not to scale.

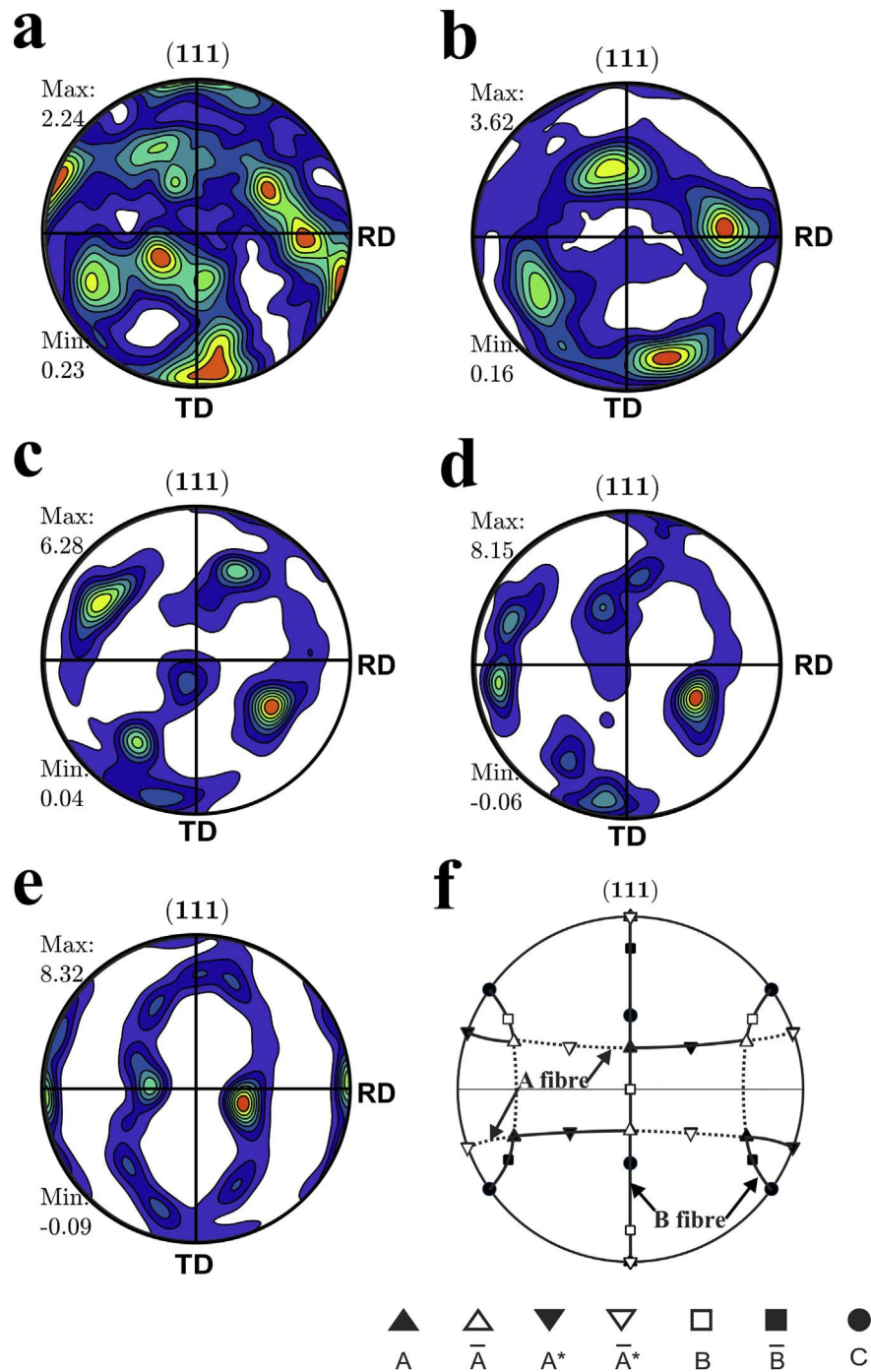


Fig. 7. (111) PF of CuCR after the tribological test. (a) 5–20 μm from the worn surface, (b) 20–50 μm , (c) 50–80 μm , (d) 110–150 μm , (e) 160–280 μm , (f) Ideal orientations for a simple shear texture.

4.2. Strain and Substructure Modification

Contrary to the very detailed local information on substructure obtained from TEM, EBSD provides substructural information in a statistical manner, by means of the misorientation angle distribution and KAM distribution. Combining these data with grain size and nano-hardness results, some interesting order-of-magnitude estimations can be made which help in the understanding of the role of strain-induced processes.

The grain size effect is generally described by the Hall-Petch relationship $\sigma_y = \sigma_0 + k_{HP}d_g^{-n}$, where an approximate equivalence between hardness H and yield stress is given as $H = 3\sigma_c$ [76–78], d_g is the

grain diameter and σ_0 , k_{HP} and n are fitting constants. Although it has been shown that the general acceptance of the value $n = 1/2$ is mainly due to imprecise statistical analysis [79,80], Cordero and Schuh have demonstrated that the more general form cited here still holds in good approximation [81]. For copper, they report values of $\sigma_0 = 40$ MPa, $k_{HP} = 160$ MPa $\cdot\mu\text{m}^n$ and $n = 0.38$. The evident deviations of this equation in Fig. 9b. can be explained by the presence of a dislocation substructure.

Dislocation density can be estimated by means of the Taylor relationship: $\sigma_y = Mab\mu\rho^{1/2}$, where the average Taylor factor M for Cu can be set equal to 3, $\alpha = 0.28$, $b = 0.28$ nm and the shear modulus $\mu = 48$ GPa. Hansen [82] proposed to superpose the strength induced

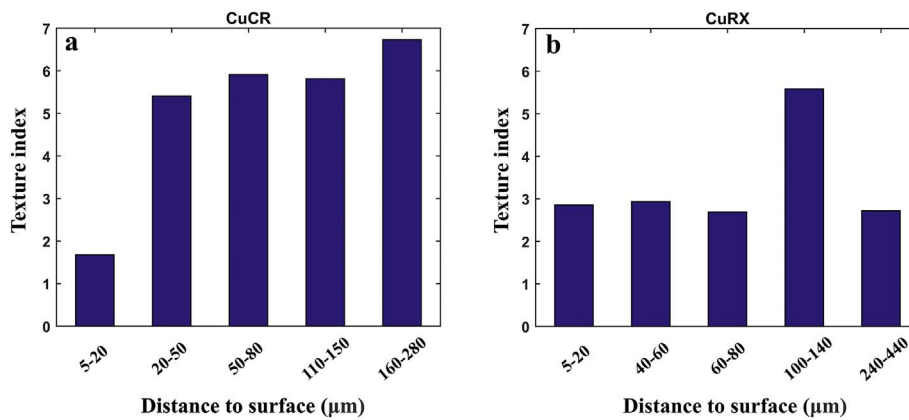


Fig. 8. Texture index corresponding to the zones shown in Fig. 7 for CuCR (a) and Fig. 4 for CuRX (b).

by dislocations and substructure on the traditional Hall-Petch relationship. A hardness of 1.4 GPa would then correspond to a dislocation density of $1.5 \times 10^{15} \text{ m}^{-2}$ in absence of grain boundaries and $4 \times 10^{14} \text{ m}^{-2}$ when the corresponding grain size of 500 nm is considered. For spherical grains, the latter value corresponds to a dislocation length of approximately 50 diameters per grain. This corresponds qualitatively to TEM-observations reported in literature [83–85], where many of the grains contain a limited quantity of forests dislocations and cell walls.

Accumulation of misorientation at the subgrain boundaries has been used to explain the creation of HAGBs in SPD [10]. The theoretical analysis of Pantleon [67] found that, for a subgrain boundary formed by the trapping of two orthogonal sets of edge dislocations, the MAD follows the Rayleigh distribution, while more complex dislocation interactions give rise to other distributions. One example is the Maxwell distribution, which was found to give a reasonable approximation for the LAGB-part of the MAD in the present work. Under this formalism, a gradual transition from the original MAD to the final one can be expected. For CuRX, one may assume that an increasing LAGB-peak would be formed, with its maximum shifting toward higher values and finally restoring a HAGB-distribution but with a much smaller grain size. For CuCR, the existing LAGB-peak should gradually shift to the right. This is not observed here: although the LAGB-peak reaches a maximum in the zone between 100 and 150 μm for both materials, a systematic shift to the right is not observed.

4.3. The Role of Recrystallisation

Recrystallisation is generally supposed to involve grain boundary movement or rearrangement. Also, while the irregular dislocation tangles, which compose the subgrain boundary may possess a complex local stress field, the grain boundaries involved in recrystallisation are

assumed to be relatively stress-free, i.e. they contain only a limited amount of extrinsic dislocations. This said, it is also clear that any recrystallisation mechanism active during the SPD-process will be affected by the ongoing strain accumulation: GBs will trap new dislocations and a new substructure can be formed inside the grain. Using statistical calculations [86], it can be estimated that up to 50% of all dislocations involved in slip will be captured at existing HAGBs for the grain size (500 nm) and dislocation densities considered in this study, with the rest contributing to substructure formation.

Static recrystallisation in severely deformed electrolytic copper can occur below 200 °C and clear evidence for recrystallisation during or after SPD-processes has been given by other authors [83–85]. For the present material and deformation mechanism, there is no doubt that recrystallisation mechanisms are active. The CuCR material shows a broad zone around 130 μm where the cold rolled material is partially recrystallised, with cube-oriented grain bands forming in a recovered matrix which inherits its crystal orientation from the cold-rolled texture. The hardness of this zone is lower than the cold-rolled substrate and the SPD top layers. It must therefore be assumed that also for these top layers, the SPD process did not start from the cold-rolled structure but from a partially or completely recrystallised state. It can also be postulated that, if the temperature and driving force are sufficient to induce recrystallisation at 130 μm in CuCR, the process will also be active in the SPD zone. Due to the low energy input from the sliding contact and the high conductivity of the copper sample and aluminium sample holder, the increased driving force close to the surface must be the principal factor in the process, as the estimated temperature increase is very low.

The misorientation angle distribution provides an argument for the importance of recrystallisation as compared to strain-induced misorientation accumulation: the measured MAD shows clear deviations from the calculated distribution. This points toward a process where

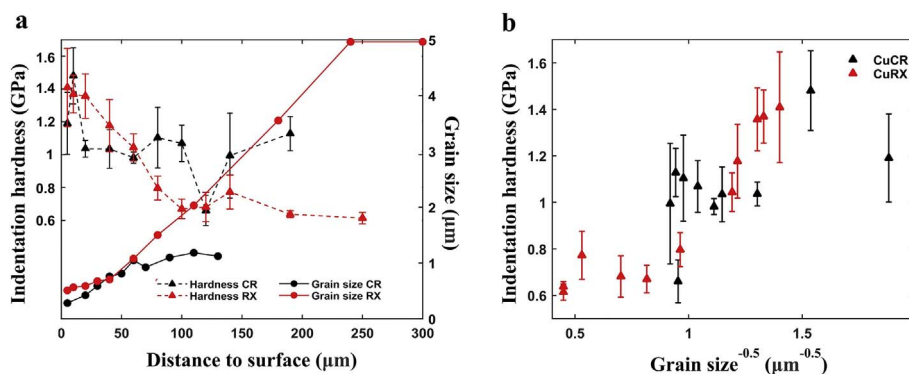


Fig. 9. (a) Chart of indentation hardness and average grain size diameter vs distance to surface, (b) dependence of hardness regarding to the inverse of square root of grain size diameter.

certain misorientations are favoured over others. Notice that, in the original description of CDRX, neither the effect of dislocations trapped at HAGBs nor the role of special GBs is considered. Strain induced misorientation accumulation is considered a CDRX mechanism but is not observed in the present work. Either, this means that CDRX is not active in the present study, or that the description of CDRX must be refined.

An activation threshold for a different mechanism is reached in the top layer of CuCR. While the zone at 25 μm in CuCR is in all aspects (MAD, KAM, grain size, hardness) comparable to the top layer in CuRX, the top layer in CuCR shows a lower hardness, lower TI, lower content of HAGB and a KAM which is almost identical to the starting material in CuRX. These elements indicate that in top layer of CuCR, the recrystallisation mechanism is faster than the effects caused by strain accumulation. This can be interpreted as dynamic recrystallisation. The reason why this threshold is reached in CuCR and not in CuRX must be sought in the smaller starting grain size observed in the partially recrystallised zone of CuCR around 130 μm .

5. Conclusions

The inverse pole figure maps presented in this study provide detailed information on the microstructural modification of electrolytically pure copper when subject to a process of sliding wear. These processes are important for the study of wear in ductile materials and the development for wear resistant materials under conditions where plastic deformation is unavoidable. Additionally, the wear test proposed here can be used deliberately as a surface modification technique.

The microstructure gradient created by the process allows studying the incremental deformation from the unaffected state in a cold-rolled or recrystallised material toward the severely deformed state at the surface. In the recrystallised sample, initial deformation introduces orientation gradients within the grains and eliminates the twin boundaries. In the cold rolled sample, a partially recrystallised zone is formed due to an increase in driving force induced by plastic deformation.

During the SPD-process, recrystallisation and deformation compete continuously. This is evidenced by three observations. Firstly, the misorientation angle distribution for low-angle grain boundaries does not show a shift toward higher angles, as expected for a purely strain-induced misorientation accumulation. Secondly, the misorientation angle distribution shows large differences with respect to the predicted one for random grain boundaries. This suggests that certain misorientations are favoured during the process. Thirdly, the hardness of the material cannot be explained by grain size or dislocation density alone but is caused by the combination of both.

Only in the top layer of the cold-rolled material, a distinct mechanism is activated. A smaller grain size is achieved but the hardness drops. The Kernel Average Misorientation is reduced to the level of the recrystallised material. Both the texture and the misorientation distribution are closer to random. This indicates that, once a certain threshold is surpassed, the recrystallisation mechanism becomes fast enough to instantly eliminate the effects of accumulated strain, i.e. a regime of dynamical recrystallisation is achieved.

Acknowledgements

CGF wishes to thank to DGAPA for his postdoctoral fellowship. RS thanks the CWO mobility fund of Ghent University for the support received during the execution of this project. This work was partially funded by DGAPA grant 114215.

References

- [1] D. Shakhvorostov, K. Pöhlmann, M. Scherge, Structure and mechanical properties of tribologically induced nanolayers, *Wear* 260 (2006) 433–437.
- [2] V. Panin, A. Kolubaev, S. Tarasov, V. Popov, Subsurface layer formation during sliding friction, *Wear* 249 (2001) 860–867.
- [3] K. Lepper, M. James, J. Chashechkina, D.A. Rigney, Sliding behavior of selected aluminum alloys, *Wear* 203–204 (1997) 46–56.
- [4] D.A. Rigney, Transfer, mixing and associated chemical and mechanical processes during the sliding of ductile materials, *Wear* 245 (2000) 1–9.
- [5] D.A. Rigney, X.Y. Fu, J.E. Hammerberg, B.L. Holian, M.L. Falk, Examples of structural evolution during sliding and shear of ductile materials, *Scr. Mater.* 49 (2003) 977–983.
- [6] A. Kapoor, Wear by plastic ratchetting, *Wear* 212 (1997) 119–130.
- [7] A. Kapoor, F.J. Franklin, Tribological layers and the wear of ductile materials, *Wear* 245 (2000) 204–215.
- [8] A. Kapoor, K.L. Johnson, Plastic ratchetting as a mechanism of metallic wear, *Proc. R. Soc. London, Ser. A* 445 (1994) 367–384.
- [9] R.Z. Valiev, I.V. Alexandrov, Nanostructured materials from severe plastic deformation, *Nanostruct. Mater.* 12 (1999) 35–40.
- [10] R.Z. Valiev, R.K. Islamgaliev, I.V. Alexandrov, Bulk nanostructured materials from severe plastic deformation, *Prog. Mater. Sci.* 45 (2000) 103–189.
- [11] R.Z. Valiev, A.V. Korznikov, R.R. Mulyukov, Structure and properties of ultrafine-grained materials produced by severe plastic deformation, *Mater. Sci. Eng. A* 168 (1993) 141–148.
- [12] J. Jiang, F.H. Stott, M.M. Stack, A mathematical model for sliding wear of metals at elevated temperatures, *Wear* 181–183 (1995) 20–31.
- [13] A. Emge, S. Karthikeyan, D.A. Rigney, The effects of sliding velocity and sliding time on nanocrystalline tribolayer development and properties in copper, *Wear* 267 (2009) 562–567.
- [14] A. Emge, S. Karthikeyan, H.J. Kim, D.A. Rigney, The effect of sliding velocity on the tribological behavior of copper, *Wear* 263 (2007) 614–618.
- [15] J. Schöfer, P. Rehbein, U. Stolz, D. Löh, K.H. Zum Gahr, Formation of tribochemical films and white layers on self-mated bearing steel surfaces in boundary lubricated sliding contact, *Wear* 248 (2001) 7–15.
- [16] A. Kapoor, F.J. Franklin, S.K. Wong, M. Ishida, Surface roughness and plastic flow in rail wheel contact, *Wear* 253 (2002) 257–264.
- [17] G. Baumann, K. Knothe, H.J. Fecht, Surface modification, corrugation and nanostructure formation of high speed railway tracks, *Nanostruct. Mater.* 9 (1997) 751–754.
- [18] W. Lojkowski, M. Djahanbakhsh, G. Bürkle, S. Gierlotka, W. Zielinski, H.J. Fecht, Nanostructure formation on the surface of railway tracks, *Mater. Sci. Eng. A* 303 (2001) 197–208.
- [19] W. Lojkowski, Y. Millman, S.I. Chugunova, I.V. Goncharova, M. Djahanbakhsh, G. Bürkle, H.J. Fecht, The mechanical properties of the nanocrystalline layer on the surface of railway tracks, *Mater. Sci. Eng. A* 303 (2001) 209–215.
- [20] W. Österle, A.I. Dmitriev, Functionality of conventional brake friction materials – perceptions from findings observed at different length scales, *Wear* 271 (2011) 2198–2207.
- [21] W. Österle, H. Kloß, I. Urban, A.I. Dmitriev, Towards a better understanding of brake friction materials, *Wear* 263 (2007) 1189–1201.
- [22] R. Schouwenaars, V.H. Jacobo, A. Ortiz, Microstructural aspects of wear in soft tribological alloys, *Wear* 263 (2007) 727–735.
- [23] W.M. Rainforth, Microstructural evolution at the worn surface: a comparison of metals and ceramics, *Wear* 245 (2000) 162–177.
- [24] R. Schouwenaars, V.H. Jacobo, A. Ortiz, Transition from normal to severe wear in PCD during high-speed cutting of a ductile material, *Int. J. Refract. Met. Hard Mater.* 27 (2009) 403–408.
- [25] W. Zein Eddine, P. Matteazzi, J.-P. Celis, Mechanical and tribological behavior of nanostructured copper–alumina cermets obtained by pulsed electric current sintering, *Wear* 297 (2013) 762–773.
- [26] Z.B. Wang, N.R. Tao, S. Li, W. Wang, G. Liu, J. Lu, K. Lu, Effect of surface nanocrystallization on friction and wear properties in low carbon steel, *Mater. Sci. Eng. A* 352 (2003) 144–149.
- [27] V.V. Stolyarov, L.S. Shuster, M.S. Migranov, R.Z. Valiev, Y.T. Zhu, Reduction of friction coefficient of ultrafine-grained CP titanium, *Mater. Sci. Eng. A* 371 (2004) 313–317.
- [28] A. Moshkovich, I. Lapsker, L. Rapoport, Correlation between strengthening and damage of Cu refined by different SPD processing and friction in different lubricant regions, *Wear* 305 (2013) 45–50.
- [29] C. Figueroa, R. Schouwenaars, V. Jacobo, A. Ortiz, R. Petrov, L. Kestens, Tribological and microstructural characterization of ultrafine layers induced by wear in ductile alloys, *Tribol. Online* 11 (2016) 389–395.
- [30] J.F. Archard, Contact and rubbing of flat surfaces, *J. Appl. Phys.* 24 (1953) 981–988.
- [31] T.H. Fang, W.L. Li, N.R. Tao, K. Lu, Revealing extraordinary intrinsic tensile plasticity in gradient nano-grained copper, *Science* 331 (2011) 1587–1590.
- [32] W.L. Li, N.R. Tao, K. Lu, Fabrication of a gradient nano-micro-structured surface layer on bulk copper by means of a surface mechanical grinding treatment, *Scr. Mater.* 59 (2008) 546–549.
- [33] N.R. Tao, Z.B. Wang, W.P. Tong, M.L. Sui, J. Lu, K. Lu, An investigation of surface nanocrystallization mechanism in Fe induced by surface mechanical attrition treatment, *Acta Mater.* 50 (2002) 4603–4616.
- [34] S.Q. Deng, A. Godfrey, W. Liu, C.L. Zhang, Microstructural evolution of pure copper subjected to friction sliding deformation at room temperature, *Mater. Sci. Eng. A* 639 (2015) 448–455.
- [35] Y. Estrin, M. Murashkin, R. Valiev, Ultrafine-grained aluminium alloys: processes, structural features and properties, in: R. Lumley (Ed.), *Fundamentals of Aluminium Metallurgy*, Woodhead Publishing, Cambridge, 2011, pp. 468–503.

[1] D. Shakhvorostov, K. Pöhlmann, M. Scherge, Structure and mechanical properties of

- [36] R.Z. Valiev, Y. Estrin, Z. Horita, T.G. Langdon, M.J. Zechetbauer, Y.T. Zhu, Producing bulk ultrafine-grained materials by severe plastic deformation, *JOM* 58 (2006) 33–39.
- [37] Y. Estrin, A. Vinogradov, Extreme grain refinement by severe plastic deformation: a wealth of challenging science, *Acta Mater.* 61 (2013) 782–817.
- [38] G. Rogl, D. Setman, E. Schafner, J. Horky, M. Kerber, M. Zehetbauer, M. Falmbigl, P. Rogl, E. Royanian, E. Bauer, High-pressure torsion, a new processing route for thermoelectrics of high ZTs by means of severe plastic deformation, *Acta Mater.* 60 (2012) 2146–2157.
- [39] K. Wang, N.R. Tao, G. Liu, J. Lu, K. Lu, Plastic strain-induced grain refinement at the nanometer scale in copper, *Acta Mater.* 54 (2006) 5281–5291.
- [40] X. Wu, N. Tao, Y. Hong, B. Xu, J. Lu, K. Lu, Microstructure and evolution of mechanically-induced ultrafine grain in surface layer of AL-alloy subjected to USSP, *Acta Mater.* 50 (2002) 2075–2084.
- [41] Y.M. Wang, M.W. Chen, H.W. Sheng, E. Ma, Nanocrystalline grain structures developed in commercial purity Cu by low-temperature cold rolling, *J. Mater. Res.* 17 (2002) 3004–3007.
- [42] A. Belyakov, T. Sakai, H. Miura, K. Tsuzaki, Grain refinement in copper under large strain deformation, *Philos. Mag. A* 81 (2001) 2629–2643.
- [43] R. Valiev, Nanostructuring of metals by severe plastic deformation for advanced properties, *Nat. Mater.* 3 (2004) 511–516.
- [44] J. Gil Sevillano, P. van Houtte, E. Aernoudt, Large strain work hardening and textures, *Prog. Mater. Sci.* 25 (1980) 69–134.
- [45] N. Hansen, New discoveries in deformed metals, *Metall. Mater. Trans. A* 32 (2001) 2917–2935.
- [46] U. Kocks, H. Mecking, Physics and phenomenology of strain hardening: the FCC case, *Prog. Mater. Sci.* 48 (2003) 171–273.
- [47] W. Pantleon, N. Hansen, Dislocation boundaries—the distribution function of disorientation angles, *Acta Mater.* 49 (2001) 1479–1493.
- [48] W. Pantleon, Stage IV work-hardening related to disorientations in dislocation structures, *Mater. Sci. Eng. A* 387–389 (2004) 257–261.
- [49] T. Sakai, A. Belyakov, R. Kaibyshev, H. Miura, J.J. Jonas, Dynamic and post-dynamic recrystallization under hot, cold and severe plastic deformation conditions, *Prog. Mater. Sci.* 60 (2014) 130–207.
- [50] A. Rollett, F. Humphreys, G.S. Rohrer, M. Hatherly, *Recrystallization and Related Annealing Phenomena*, Elsevier, Amsterdam, 2004.
- [51] R.D. Doherty, D.A. Hughes, F.J. Humphreys, J.J. Jonas, D.J. Jensen, M.E. Kassner, W.E. King, T.R. McNelley, H.J. McQueen, A.D. Rollett, Current issues in recrystallization: a review, *Mater. Sci. Eng. A* 238 (1997) 219–274.
- [52] A.A. Nazarov, A.E. Romanov, R.Z. Valiev, On the structure, stress fields and energy of nonequilibrium grain boundaries, *Acta Metall. Mater.* 41 (1993) 1033–1040.
- [53] R.Z. Valiev, I.V. Alexandrov, Y.T. Zhu, T.C. Lowe, Paradox of strength and ductility in metals processed by severe plastic deformation, *J. Mater. Res.* 17 (2002) 5–8.
- [54] R. Valiev, Materials science: nanomaterial advantage, *Nature* 419 (2002) 887–889.
- [55] L.S. Toth, C. Gu, Ultrafine-grain metals by severe plastic deformation, *Mater. Charact.* 92 (2014) 1–14.
- [56] I.J. Beyerlein, L.S. Tóth, Texture evolution in equal-channel angular extrusion, *Prog. Mater. Sci.* 54 (2009) 427–510.
- [57] G.R. Canova, U.F. Kocks, J.J. Jonas, Theory of torsion texture development, *Acta Metall.* 32 (1984) 211–226.
- [58] F. Montheillet, M. Cohen, J.J. Jonas, Axial stresses and texture development during the torsion testing of Al, Cu and α -Fe, *Acta Metall.* 32 (1984) 2077–2089.
- [59] L.S. Toth, P. Gilormini, J.J. Jonas, Effect of rate sensitivity on the stability of torsion textures, *Acta Metall.* 36 (1988) 3077–3091.
- [60] L.S. Toth, J.J. Jonas, D. Daniel, J.A. Bailey, Texture development and length changes in copper bars subjected to free end torsion, *Textures Microstruct.* 19 (1992) 245–262.
- [61] S. Suwas, R.K. Ray, *Crystallographic Texture of Materials*, Springer, 2014.
- [62] N.A. Enikeev, E. Schafner, M.J. Zehetbauer, I.V. Alexandrov, R. Valiev, Observations of texture in large scale HPT-processed Cu, *Mater. Sci. Forum* 584 (2008) 367–374.
- [63] C. Figueroa, I. Ortega, V. Jacobo, A. Ortiz, A. Bravo, R. Schouwenaars, Microstructures of tribologically modified surface layers in two-phase alloys, *IOP Conf. Ser.: Mater. Sci. Eng.* 63 (2014) 012018.
- [64] C.G. Figueroa, V.H. Jacobo, A. Ortiz, R. Schouwenaars, Critical analysis of a coaxial configuration for the characterization of adhesive wear and its application to Al and Al–Sn alloys, *Tribol. Lett.* 59 (2015) 14.
- [65] F. Bachmann, R. Hielscher, H. Schaeben, Texture analysis with MTEX—free and open source software toolbox, *Sol. St. Phen.* 160 (2010) 63–68.
- [66] L.S. Toth, C.F. Gu, B. Beausir, J.J. Fundenberger, M. Hoffman, Geometrically necessary dislocations favor the Taylor uniform deformation mode in ultra-fine-grained polycrystals, *Acta Mater.* 117 (2016) 35–42.
- [67] W. Pantleon, On the statistical origin of disorientations in dislocation structures, *Acta Mater.* 46 (1998) 451–456.
- [68] W.C. Oliver, G.M. Pharr, An improved technique for determining hardness and elastic modulus using load and displacement sensing indentation experiments, *J. Mater. Res.* 7 (1992) 1564–1583.
- [69] W.C. Oliver, G.M. Pharr, Measurement of hardness and elastic modulus by instrumented indentation: advances in understanding and refinements to methodology, *J. Mater. Res.* 19 (2004) 3–20.
- [70] K. Kese, Z. Li, B. Bergman, Influence of residual stress on elastic modulus and hardness of soda-lime glass measured by nanoindentation, *J. Mater. Res.* 19 (2004) 3109–3119.
- [71] K. Kese, Z.-C. Li, Semi-ellipse method for accounting for the pile-up contact area during nanoindentation with the Berkovich indenter, *Scr. Mater.* 55 (2006) 699–702.
- [72] K. Kese, Z.-C. Li, B. Bergman, Method to account for true contact area in soda-lime glass during nanoindentation with the Berkovich tip, *Mater. Sci. Eng. A* 404 (2005) 1–8.
- [73] X. Sauvage, G. Wilde, S.V. Divinski, Z. Horita, R.Z. Valiev, Grain boundaries in ultrafine grained materials processed by severe plastic deformation and related phenomena, *Mater. Sci. Eng. A* 540 (2012) 1–12.
- [74] L.S. Toth, K.W. Neale, J.J. Jonas, Stress response and persistence characteristics of the ideal orientations of shear textures, *Acta Metall.* 37 (1989) 2197–2210.
- [75] A. Kapoor, F.J. Franklin, Tribological layers and the wear of ductile materials, *Wear* 245 (2000) 204–215.
- [76] K.L. Johnson, *Contact Mechanics*, Cambridge University Press, 1985.
- [77] D. Tabor, *The Hardness of Metals*, Oxford University Press, 2000.
- [78] D. Tabor, The hardness of solids, *Rev. Phys. Technol.* 1 (1970) 145.
- [79] W.M. Baldwin, Yield strength of metals as a function of grain size, *Acta Metall.* 6 (1958) 139–141.
- [80] D.J. Dunstan, A.J. Bushby, The scaling exponent in the size effect of small scale plastic deformation, *Int. J. Plast.* 40 (2013) 152–162.
- [81] Z.C. Cordero, B.E. Knight, C.A. Schuh, Six decades of the Hall–Petch effect – a survey of grain-size strengthening studies on pure metals, *Int. Mater. Rev.* 61 (2016) 495–512.
- [82] N. Hansen, Hall–Petch relation and boundary strengthening, *Scr. Mater.* 51 (2004) 801–806.
- [83] N. Lugo, N. Llorca, J.M. Cabrera, Z. Horita, Microstructures and mechanical properties of pure copper deformed severely by equal-channel angular pressing and high pressure torsion, *Mater. Sci. Eng. A* 477 (2008) 366–371.
- [84] T.L. Brown, C. Saldana, T.G. Murthy, J.B. Mann, Y. Guo, L.F. Allard, A.H. King, W.D. Compton, K.P. Trumble, S. Chandrasekar, A study of the interactive effects of strain, strain rate and temperature in severe plastic deformation of copper, *Acta Mater.* 57 (2009) 5491–5500.
- [85] W.H. Huang, C.Y. Yu, P.W. Kao, C.P. Chang, The effect of strain path and temperature on the microstructure developed in copper processed by ECAE, *Mater. Sci. Eng. A* 366 (2004) 221–228.
- [86] R. Schouwenaars, M. Seefeldt, P.V. Houtte, A probabilistic derivation of the effect of grain size on the dislocation free path in a deforming polycrystal, *Scr. Mater.* 62 (2010) 590–593.